Ravi, S. K., Zhang, Y., Wang, Y., Nandakumar, D. K., Sun, W., Jones, M. R., & Tan, S. C. (2019). Optical Shading Induces an In-Plane Potential Gradient in a Semiartificial Photosynthetic System Bringing Photoelectric Synergy. *Advanced Energy Materials*, *9*(35), [1901449]. https://doi.org/10.1002/aenm.201901449

Optical-shading-induced In-plane Potential Gradient Creates a Photoelectric Synergy in a Semi-artificial Photosynthetic System

Sai Kishore Ravi[1], Yaoxin Zhang[1], Yanan Wang[1], Dilip Krishna Nandakumar[1], Wanxin Sun[2], Michael R. Jones[3], Swee Ching Tan[1]*

[1]Department of Materials Science and Engineering, National University of Singapore, 9 Engineering Drive 1, Singapore 117575.

[2]Bruker Nano Surface Division, 11 Biopolis Way #10-10, The Helios, Singapore 138667.

[3]School of Biochemistry, University of Bristol, Biomedical Sciences Building, University Walk, Bristol BS8 1TD, United Kingdom.

*Correspondence to: msetansc@nus.edu.sg

Abstract

Semi-artificial photosynthetic systems have opened up new avenues for harvesting solar energy using natural photosynthetic materials in combination with synthetic components. In this work, we report a new, semi-artificial system for solar energy conversion that synergistically combines photoreactions in a purple-bacterial photosynthetic membrane with those in three types of transition metal-semiconductor Schottky junctions. An optically transparent film of a common transition metal interfaced with an n-doped silicon semiconductor exhibited an in-plane potential gradient under illumination when its surface was partially shaded by a multilayer of highly-absorbing membranes from a photosynthetic bacterium capable of generating a photocurrent. Electrical connection to a transparent front electrode was enhanced using a biocompatible thixotropic gel electrolyte that permeated the membrane multilayer. In-plane potential gradients in the range of 0.08 to 0.3 V synergistically enhanced charge transport in the system, driving a strong and steady photoelectric current of up to 1.3 mA cm^{-2}.

Introduction

Tapping sunlight economically and efficiently for diverse applications is one of the grand challenges of this century. With new developments in materials and methods for the conversion of solar energy into electric power and chemical fuels, photovoltaic and photoelectrochemical technologies are rapidly progressing and are believed to be key to sustainably overcoming the terawatt energy challenge the world currently faces[1, 2]. The field of solar energy harvesting, previously dominated by inorganic materials, has in recent times witnessed the rapid ascent of organic materials in device designs[3]. In particular, much of the progress in this field has been driven by bio-inspiration with nature's photosynthetic apparatus as a model material[4, 5, 6]. The aim of exploiting nature's designs for the harnessing of solar energy has attracted considerable efforts in the areas of artificial photosynthesis[7, 8], bio-photovoltaics and bio-electrochemical cells[6, 9, 10, 11]. The '*biomimetic solar cell*', an application long-sought-after, aims to mimic the architecture of nature's reaction centre (RC) and light-harvesting (LH) complexes in a fully artificial photosynthetic device for direct '*solar electricity*' generation[12]. Although the basic design principle of a dye-sensitized solar cell comes closer to this idea[13], it is undeniably far from having any structural similarity with photosynthetic proteins, and developing supramolecular solar cells with artificial RCs[14] or other protein-mimics has been extremely challenging[15]. Alongside the development of artificial photosynthetic systems, there have also been attempts to directly employ natural photosynthetic materials such as bacterial cells[16, 17, 18], pigment-proteins[19, 20, 21, 22, 23, 24] and membranes[25, 26] as photoactive components for both direct electricity generation and fuel molecule synthesis.

While on the one hand fully artificial photosynthetic systems lack the nanoscale architectural sophistication found in natural photosystems, on the other hand natural photosystems are not always sufficiently robust or efficient outside their native environments. These and other factors limit the performance of a device employing solely natural or artificial materials as the photoactive component[27]. Bridging the two approaches, the idea of semi-artificial photosynthetic systems is now gaining attention as it offers advantages over purely artificial or biological systems[27, 28]. The concept has already shown signs of success in fuel generation by photoelectrochemical water splitting[29, 30]. Direct electric current generation has also been studied in a wide variety of bio-hybrid devices, combining different photosynthetic microorganisms[16 17, 31] and enzymes/proteins[19, 20, 21, 32, 33, 34, 35, 36, 37, 38, 39, 40, 41, 42, 43] with diverse synthetic materials including bulk-semiconductors[44, 45], semiconductive nanowires[46, 47], quantum dots[48], and plasmonic metal nano-structures[40, 49]. Despite progress in this area a photo-electric synergy between synthetic and biological components has not been fully established. Unlike the simple additive effect of photocurrent enhancement seen, for example, in bio-hybrid tandem cells[50], a synergistic effect that yields a photocurrent that is more than just the sum of photocurrents from the individual photoactive components is a possible advantage of a semi-artificial photosynthetic system.

In this work we demonstrate the generation of a high electric current in a synergistic, semi-artificial photosynthetic system comprising a multilayer of membrane fragments from a purple photosynthetic bacterium that partially covers a Schottky junction

formed at the interface of a transition metal and a semiconductor. Central to the synergy displayed by this system is the optical generation of an in-plane potential gradient in the metal layer that greatly enhances photocurrent generation by the natural membranes (**Figure 1**). In-plane electric fields have recently been found to be vital in controlling and manipulating the dynamics and distribution of photoexcited charges in doped semiconductors[51]. In the present case the in-plane potential gradient gives rise to increased directional charge transport between electrodes facilitated by the photosynthetic membranes and a permeating gel-phase electrolyte. Kelvin Probe Force Microscopy (KPFM) is used to characterise light-induced surface potential shifts in the membrane multilayer and in three types of Schottky junction formed between n-doped silicon and copper, nickel or molybdenum. Based on the in-plane potential gradient established beween different areas of these metal/Si Schottky electrodes on illumination, a proof-of-concept "Bio-Schottky cell" is constructed employing a bio-compatible thixotropic gel electrolyte which generated a stable electric current of up to 1.3 mA cm^{-2}. To our knowledge, this is the highest photocurrent reported for any biohybrid device based on exposure of the purple bacterial photosynthetic apparatus to standard illumination.

Results

Establishment of an In-plane Potential Gradient on a Bio-Schottky Electrode

To demonstrate the feasibility of using photosynthetic membranes to form a Bio-Schottky cell we first examined the individual photoresponses of the membrane and Schottky junction components (see Materials and Methods). For the former a highly-absorbing film was formed by drop-casting 10 µl of a concentrated solution of membrane fragments on a glass substrate and partially drying under vacuum. This process did not change the absorption characteristics of the membrane film compared to membranes in solution, confirming that the *Rhodobacter* (*Rba.*) *sphaeroides* RC-LH1 complexes that made up these membranes were structurally intact (**Figure S1A, Supplementary Information**). Atomic force microscopy of the resulting film surface (**Figure 2A**) showed a non-uniform topology that included areas displaying ring structures of the expected diameter for *Rba. sphaeroides* RC-LH1 proteins (≈13 nm), consistent with a multilayer film formed from randomly-deposited membrane fragments. The surface potential of a 40,000 nm^2 area of the film was then mapped using KPFM either in the dark or when illuminated by white light (20 mW cm^{-2}). The shift in surface potential on illumination was characterized from the change in contact potential difference (V_{CPD}) between the film and a Pt-Ir probe of known surface potential (**Figure 2B**). Under either illumination condition the surface potential map was non-uniform (**Figure 2C,D**), consistent with the non-uniform nature of the membrane fragment multilayer (**Figure 2A**). In the dark, the contact potential difference was distributed around ≈810 mV (**Figure 2C,E**), but when illuminated this distribution shifted by ≈30 mV (**Figure 2D,E**). This and other (see below) illumination-induced surface potential shifts were quantified as the separation between mode values of the V_{CPD} distributions measured under dark and illuminated conditions (**Figure 2E**).

This change can be attributed solely to the photoactivity of the RC-LH1 complexes in the photosynthetic membranes (blue electrons in **Figures 1A and 2B**) as they were the sole photoactive component in this partial system. Information on the structure of RC-LH1 complexes and the mechanism of photochemical charge separation is given in **Figure S1B,C Supplementary Information**.

KPFM was also used to examine the photoactivity of fabricated Cu/Si, Mo/Si and Ni/Si substrates (see Materials and Methods). For all three the interface of the metal and the semiconductor was confirmed to be a Schottky junction from its current-voltage (*IV*) profile (**Figure S2, Supplementary Information**). Example surface potential maps recorded for 60 s in the dark and 60 s under illumination are shown in **Figure 3A-C**; these produced light-induced surface potential shifts (mode-to-mode) of 275 mV for Cu/Si, 200 mV for Mo/Si and 85 mV for Ni/Si. The statistical range of the light-induced surface potential shifts from repeat measurements of the three types of Schottky electrode is presented in **Figure 3D**. The Cu/Si system produced an average surface potential shift of 256 mV and a maximum mode-to-mode shift in an individual measurement of 310 mV (**Figure S3A**, **Supplementary Information**). To our knowledge, light-induced surface potential shifts reported for metal thin films to date have not previously exceeded 220 mV[52].

The surface potential shift displayed by these Schottky electrodes can manifest as an in-plane potential gradient if a light-intensity gradient is induced on the metal surface. As concentrated photosynthetic membranes are highly absorbing, deposition of a thick film on part of a Schottky electrode should shade that region from photoexcitation, producing distinct zones with different surface potentials under illumination (**Figure 3E**). Such composite membrane/metal/semiconductor electrodes were fabricated by drop-casting and vacuum drying a membrane film on part of the metal surface (see Materials and Methods) and the potential difference between coated and uncoated zones measured under illumination (**Figure 3E**). The maximum in-plane potential gradients on the Cu, Mo and Ni electrodes were 218 mV, 95 mV and 14 mV respectively (**Figure 3F**), their sizes following the same dependence on metal type as the surface potential shifts measured using KPFM.

Enhanced Charge Transfer by Thixotropic Electrolytes

To build a Bio-Schottky photoelectrochemical cell a quasi-solid-state electrolyte was developed to connect the currents generated by the photosynthetic membrane and Schottky junction systems to a transparent aluminium-doped zinc oxide (AZO)-glass counter electrode. To form a solid-state electrolyte interface with a thermally labile material such as a photosynthetic membrane is challenging as most electrolyte matrices require heating to a temperature above 80 °C for liquefaction before adding to the photoactive layer to form a solid-state interface on cooling. As such heating would damage photosynthetic proteins and membranes a thixotropic electrolyte was developed that could be liquefied at room temperature by sonicating, and which solidified on resting. This was based on succinonitrile (SN), a plastic crystalline material[53] that has been used

as a matrix for electrolytes in solid-state photovoltaics and batteries[54, 55]. SN is typically liquefied by heating, but in a recent report SN doped with a disulfide-thiolate redox couple was found to liquify by a mechanical stimulus at room temperature[20]. In the present work, gels formed from simple mixtures of SN and water were also found to exhibit thixotropy.

The phases formed by mixtures of water:SN varying from 1:100 to 7:100 (v/v) are illustrated in **Figure 4A**. At 1:100 or lower the mixture was solid and could not be liquefied by sonication at room temperature, whilst at 6:100 and above the mixtures were liquid at room temperature. Intermediate compositions were a gel at room temperature but transiently underwent a thixotrophic conversion to a liquid in response to sonication. From rheological measurements it was found that the higher the volume of water in the gel, the lower was its viscosity both in the solid and liquid states (**Figure 4B**). The shear strain required for the solid-to-liquid phase change decreased with increasing water content (**Figure S4 in Supplementary Information)** with the practical consequence that the sonication time required to effect the phase change also shortened (**Figure 4C**).

Mixtures with water:SN ratios ranging from 2:100 to 4:100 were used as the electrolyte matrices as they formed relatively stable gel phases that, unlike the 5:100 mixture, were not prone to turn liquid in response to gentle vibration. Ubiquinone-0 (Q0) was used as the electron transport mediator and was suffused into the liquid-state of the sonicated gel to a final concentration of 80 mM (**Figure 4D**). Q0 is a water-soluble analogue of ubiquinone-10 which is the natural electron acceptor for the RC-LH1 complex. The resulting formulations remained thixotropic and exhibited good reversibility between the solid and the liquid states (**Figure S5, Supplementary Information**).

To apply the electrolyte, 5 µl of sonicated Q0-SN was deposited on the membrane film partially covering a Schottky electrode. The sonicated electrolyte, being initially in a liquid state, soaked into the air-dried photosynthetic membrane film and within a few minutes of rest formed a stable solid-state interface for connection of the membrane multilayer to a counter electrode. To verify that the Q0-SN gel was performing the role of an electrolyte, KPFM was applied to a film of membranes mixed with Q0-SN electrolyte on a glass substrate. A surface potential shift of 43 mV was observed under illumination **(Figure S6, Supplementary Information**), significantly higher than the 30 mV shift obtained in the absence of the electrolyte **(Figure 2E)**. This was consistent with charge movement by the electrolyte under illumination.

KPFM was also applied to membrane films coated on Schottky electrodes (**Figure 5A**) either without **(Figure 5B,C**) or with (**Figure 5D-F**) the Q0-SN gel. The average illumination-induced surface potential shift for several Cu/Si electrodes with Q0-SN (159 mV – **Figure 5G**) was almost double that seen when the electrolyte was absent (83 mV). Thus both the absolute level of surface potential shift and the enhancement caused by the electrolyte was geater when membranes were coated on Cu/Si than on glass (**Figure 5G**). Measurements on a 200 x 200 nm area of membrane/Q0-SN composite film coated on Cu/Si gave an illumination-induced surface potential shift of 174 mV (**Figure S7 Supplementary Information**) which was in reasonably good agreement with the in-plane surface potential gradient of 218 mV determined for a partially membrane-coated Cu/Si

electrode (**Figure 3F**). Similarly, the microscopic surface potential shift of 105 mV observed for a membrane/Q0-SN composite film coated on Mo/Si (**Figure S8A-C Supplementary Information**) was in good agreement with the measured in-plane potential gradient of 95 mV for a partially membrane-coated Mo/Si electrode (**Figure 3F**). This showed that the surface potential shift measured for the Bio-Schottky electrode system was a function of both the type of underlying Schottky electrode and the presence of the Q0-SN mediator (**Figure 5H**).

To rule out the possiblity of any individual photo-electric contribution from the metal surface, independent of the Schottky junction, the surface potential of a membrane/Q0-SN composite film coated on a Cu foil surface was also examined (**Figure S9, Supporting Information**). A surface potential shift of 50 mV was observed on illumination, close to that obtained with the same composite film on glass (**Figure 5G**). This demonstrated that a large surface potential shift could only be obtained when Cu formed part of a Schottky junction capable of generating an in-plane surface potential gradient (**Figure 5H**).

Synergistic Photo-electric Effect in Bio-Schottky Cells

Photocurrent generation by complete Bio-Schottky cells with a transparent AZO-glass counter electrode was measured under white light illumination (**Figure 6A**). Cells based on Cu/Si electrodes generated the highest photocurrent density in the range of 1.13 mA cm^{-2} to 1.32 mA cm^{-2}, followed by Mo/Si cells with 0.9-0.94 mA cm^{-2} and Ni/Si cells with 0.7-0.74 mA cm^{-2}, in accord with the trends seen for the light-induced surface potential shifts (**Figure 3D**) and in-plane potential gradients (**Figure 3F**). A control cell with a Cu/Si Schottky junction and electrolyte but no photosynthetic membranes generated a negligible photocurrent of ≈0.005 mA cm^{-2}, proving the key role played by the photoproteins in photocurrent generation (**Figure 6B**). Photocurrents generated by the Bio-Schottky cells were also significantly higher than those obtained from cells in which the Schottky junction was replaced by an ohmic contact between Cu and an FTO-glass substrate (0.2 mA cm^{-2} - **Figure 6B**). In contrast to the sharp photoresponses displayed by the Bio-Schottky cells (**Figure 6A,B**), these bio-hybrid “non-Schottky” cells displayed a slow photocurrent increase upon ‘light ON’ and a gradual current decay upon ‘light OFF’ (**Figure 6C**). This can be attributed to sluggish charge transport in the absence of an in-plane potential gradient to provide a strong driving force for electron flow.

To check the maximum photocurrent generation possible with just a standalone Schottky junction without any electrolytes or photoproteins, the Cu/Si system was tested as a conventional Schottky junction solar cell with one device terminal attached to the Cu and the other to the n-Si. These “non-bio” Schottky cells generated a maximum of 0.3 mA cm^{-2} when illuminated through the metal film and around half of this when illuminated from from the n-Si side (**Figure 6D**). Thus, as illustrated in **Figure 6E**, the photocurrent produced by the Bio-Scottky cell was more than twice the sum of the photocurrents produced by a non-bio Schottky cell and a bio-hybrid non-Schottky cell, a synergistic effect achieved by combining the photosynthetic membrane/electrolyte component with

the Schottky junction component to harness the in-plane potential gradient between the two.

Discussion

Most metals will form a Schottky contact with n-Si as a result of the band-bending in the semiconductor, producing an energy barrier at the metal/semiconductor interface characterised by a Schottky barrier height (SBH). This barrier is typically overcome by photon irradiation enabling electron injection from the semiconductor conduction band to the metal, and Schottky junction solar cells have been developed based on this concept. In the Bio-Schottky cells described here, the band structures of two distinct zones are relevant to the working mechanism of the device. In 'Zone 1' (**Figure 7A**) the Schottky junction electrode is shaded by a thick, optically-opaque membrane multilayer film that prevents photoexcitation of the underlying semiconductor. This leaves the surface of the metal film at its ground-state potential as there is no injection of electrons from the n-Si conduction band into the metal. In Zone 2 (**Figure 7B**) the lack of a membrane film means that almost 80% of the incident light reaches the Schottky junction inducing photoexcitation of the n-Si. Under continuous illumination, as photoexcited electrons keep accumulating in the conduction band of the n-Si, those near the barrier with sufficient kinetic energy (known as "hot electrons"[52]) jump into the metal layer, increasing its surface potential. The continuous nature of the two zones results in a lateral surface potential gradient which drives a flow of electrons from the zone of higher surface potential to the zone with lower surface potential (**Figure 7C**).

The overall mechanism of photocurrent generation by a Bio-Schottky cell is summarised in **Figure 7D**. When the device is illuminated the membrane-embedded RC-LH1 photoproteins in Zone 1 and the Schottky junction in Zone 2 simultaneously undergo photoexcitation to create a pigment excited electronic state in the former (P*) and hot electrons in the latter (rainbow arrows). Charge separation in the photoprotein (dotted arrows) leaves a positive charge at the special pair of bacteriochlorophylls (P^+) and a negative charge at the ubiquinone (Q_B^-) (see **Figure S1C** in **Supplementary Information** for details). The Q0-SN electrolyte shuttles the electrons from the Q_B^- site to the AZO electrode (blue arrows). The photo-oxidized P^+ in the photoprotein is reduced by electrons from the outer circuit reaching the Schottky electrode in Zone 1 and by photoexcited electrons in Zone 2 of the Schottky electrode that flow down-hill into Zone 1 (dark blue arrows). The photogenerated electrons at the Schottky electrode also are transported to the front electrode directly by the electrolyte, adding to the photocurrent (**Figure 7D**, green arrow).

Surface potential shifts dependent on illumination intensity have recently been established in Au/Si and Pt/Si Schottky systems[52]. The present work used more abundant and lower cost transition metals, and achieved, in the case of Cu, a higher in-plane potential gradient. In addition aluminium-doped zinc oxide was used as a transparent conductive coating for the front electrode, enabling the fabrication of a photoelectrochemical cell without the use of precious or low-abundance metal

components. Intact membranes were employed as the biological component rather than the purified proteins used in our previous work on photosynthetic multilayers[20]; this simplified biochemical purification and avoided the use of expensive detergents, greatly saving on both production time and cost. To increase the density of charge separating RCs in the *Rba. sphaeroides* membranes, genetic engineering was used to remove the normally-dominant LH2 light harvesting protein, and the PufX protein was also removed to maximise the size of the LH1 light harvesting protein within each RC-LH1 complex[56]. The latter change also converted the morphology of the photosynthetic membrane from the spheres seen in the presence of LH2 and the long tubes seen in its absence to flat sheets in which RC-LH1 complexes were arranged in hexagonally-packed arrays[57], enabling the preparation of membrane fragments with good access for a permeating mediator to either side of the membrane. Finally, electrical coupling to either electrode was enhanced using a gel electrolyte that could be suffused through the membrane multilayer in a non-damaging manner through a sonication-induced phase-change. The role of this electrolyte was critical in effectively transporting the photogenerated electrons from the photosynthetic proteins and the underlying Schottky electrode to the AZO-glass front electrode, forming a potential difference across the device similar in magnitude to that of the in-plane surface potential gradient.

In summary, we demonstrate the construction of a semi-artificial photosynthetic system that exploits an in-plane surface potential gradient to generate a high electric current in response to solar illumination. This combination of natural and synthetic photoactive components exhibited a synergistic photo-electric effect with a current output as high as 1.3 mA cm^{-2}. Photocurrents reported so far from biohybrids based on purple-bacterial photosynthetic systems have typically been in the range of tens to hundreds of microamperes and have never exceeded 1 mA cm^{-2} under standard illumination. In addition to the high performance, this semi-artificial system casts new light on combining well-studied inorganic systems with natural photosynthetic systems using biocompatible fabrication procedures. Besides its application in biohybrids, the effect of the in-plane surface potential gradient should have wide applicability in other optoelectronic and photovoltaic devices involving light-intensity gradients.

Methods

Biological Material

Photosynthetic membranes were prepared from a strain of *Rba. sphaeroides* lacking the peripheral LH2 light harvesting complex and the PufX protein[50, 56]. Bacterial cells were grown under semiaerobic conditions in the dark and harvested by centrifugation[58]. Cells resuspended in 20 mM Tris (pH 8.0) were lysed in a Constant Systems Cell Disruptor, unbroken cells removed by centrifugation (18,000 rpm, 4°C, 20 min) and membrane fragments isolated on one step density gradients formed from equal volumes of 40 % and 15 % (w/v) sucrose in 20 mM Tris (pH 8.0) that were ultracentrifuged at 38,000 rpm and 4°C for 20 min. Membrane fragments accumulated at the gradient interface were diluted in 20 mM Tris (pH 8.0), pelleted by ultracentrifugation (38,000 rpm, 4°C, 20 min) and resuspended by homogenisation in a minimal volume of 20 mM Tris (pH 8.0). The final concentrated solution had an absorbance at 875 nm of approximately 200 absorbance units cm^{-1} and was aliquoted and stored at -80°C until use. The membrane fragments contained the PufX-deficient RC-LH1 complex as the sole photosynthetic protein.

Schottky Electrode Fabrication

Precleaned n-type silicon wafers (prime grade, 525 µm thick, 3 cm^2 in area) were coated with Cu, Mo, or Ni by using magnetron sputtering to an approximately equal thickness (≈ 13 ± 2 nm) producing an optical transmittance of 80 ± 3%.

Electrolyte Preparation and Rheological Measurements

Succinonitrile was heated to 80 °C and gels with different volume fractions of water were prepared by adding water to molten succinonitrile before cooling to room temperature. The gels exhibiting thixotropy (i.e. those with a water:SN volume ratio between 2:100 and 4:100) were sonicated for less than a minute to liquefy the gel. Ubiquinone Q0 was added to liquified gels with stirring at room temperature to a concentration of 80 mM. All thixotropic gels returned to the solid form within one hour of resting at room temperature. Rheological measurements were conducted using a MCR 702 TwinDrive Rheometer (Anton Paar).

Device Fabrication

A 10 µL aliquot of concentrated membrane solution was drop-cast onto part of a metal-coated n-type Si wafer and vacuum dried to form a patch of ~3 mm in diameter with a maximum thickness of 300 µm and 0 % transmittance. The Q0-SN gel electrolyte was liquefied by sonication and 5 µL was added to the membrane film and allowed to soak in. The electrolyte was allowed to rest for 15 minutes at room temperature to ensure a solid-state interface between the membranes and the electrolyte, after which an AZO-coated glass electrode was placed on top to form the final cell.

Microscopic Surface Potential Scans

Surface potential scans were carried out by KPFM using a Dimension Icon microscope (Bruker Nano Surface, Santa Barbara, CA). An amplitude modulation mode was employed to obtain a high signal-to-noise ratio and measurements were performed in a dual pass mode to eliminate topography effects. Pt/Ir coated SCM-PIT probes (Bruker) with an applied bias were used to probe the surface potentials of the metal and photosynthetic membrane films. Illumination-induced surface potential shifts were determined from changes in the contact potential difference (CPD) between the tip and the sample with and without illumination from a tungsten-halogen lamp with an incident light intensity of 20 mW cm^{-2}.

Electrical Measurements

Photocurrent measurements were carried out using a Keithley K2450 source meter. Illumination was provided using a tungsten-halogen lamp providing an incident light intensity of 100 mW cm^{-2}, approximating to 1 sun illumination, applied to an area of 4 mm^2.

Data availability

All relevant data will be made available upon reasonable request. Requests for data should be addressed to S.C.T

References:

1. Cheng P, Li G, Zhan X, Yang Y. Next-generation organic photovoltaics based on non-fullerene acceptors. *Nature Photonics* **12**, 131 (2018).

2. Huang W, Cheng P, Yang Y, Li G, Yang Y. High-Performance Organic Bulk-Heterojunction Solar Cells Based on Multiple-Donor or Multiple-Acceptor Components. *Advanced Materials* **30**, 1705706 (2018).

3. Leo K. Organic photovoltaics. *Nature Reviews Materials* **1**, 16056 (2016).

4. Bredas JL, Sargent EH, Scholes GD. Photovoltaic concepts inspired by coherence effects in photosynthetic systems. *Nat Mater* **16**, 35-44 (2017).

5. Barber J. Photosynthetic energy conversion: natural and artificial. *Chemical Society Reviews* **38**, 185-196 (2009).

6. Ravi SK, Tan SC. Progress and perspectives in exploiting photosynthetic biomolecules for solar energy harnessing. *Energy & Environmental Science* **8**, 2551-2573 (2015).

7. Berardi S, Drouet S, Francas L, Gimbert-Suriñach C, Guttentag M, Richmond C, Stoll T, Llobet A. Molecular artificial photosynthesis. *Chemical Society Reviews* **43**, 7501-7519 (2014).

8. Lewis NS. Developing a scalable artificial photosynthesis technology through nanomaterials by design. *Nature nanotechnology* **11**, 1010 (2016).

9. Ravi SK, Udayagiri VS, Suresh L, Tan SC. Emerging Role of the Band-Structure Approach in Biohybrid Photovoltaics: A Path Beyond Bioelectrochemistry. *Advanced Functional Materials* **28**, 1705305 (2018).

10. McCormick AJ, Bombelli P, Bradley RW, Thorne R, Wenzel T, Howe CJ. Biophotovoltaics: oxygenic photosynthetic organisms in the world of bioelectrochemical systems. *Energy & Environmental Science* **8**, 1092-1109 (2015).

11. Friebe VM, Frese RN. Photosynthetic reaction center-based biophotovoltaics. *Current Opinion in Electrochemistry* **5**, 126-134 (2017).

12. Gust D, Moore TA, Moore AL. Mimicking photosynthetic solar energy transduction. *Accounts of Chemical Research* **34**, 40-48 (2001).

13. McConnell R. Assessment of the dye-sensitized solar cell. *Renewable and sustainable energy reviews* **6**, 271-293 (2002).

14. Kuciauskas D, Liddell PA, Lin S, Johnson TE, Weghorn SJ, Lindsey JS, Moore AL, Moore TA, Gust D. An artificial photosynthetic antenna-reaction center complex. *Journal of the American Chemical Society* **121**, 8604-8614 (1999).

15. Hasobe T, Kashiwagi Y, Absalom MA, Sly J, Hosomizu K, Crossley MJ, Imahori H, Kamat PV, Fukuzumi S. Supramolecular photovoltaic cells using porphyrin dendrimers and fullerene. *Advanced Materials* **16**, 975-979 (2004).

16. Saper G, Kallmann D, Conzuelo F, Zhao F, Tóth TN, Liveanu V, Meir S, Szymanski J, Aharoni A, Schuhmann W. Live cyanobacteria produce photocurrent and hydrogen using both the respiratory and photosynthetic systems. *Nature communications* **9**, 2168 (2018).

17. Wenzel T, Härtter D, Bombelli P, Howe CJ, Steiner U. Porous translucent electrodes enhance current generation from photosynthetic biofilms. *Nature communications* **9**, 1299 (2018).

18. Saar KL, Bombelli P, Lea-Smith DJ, Call T, Aro E-M, Müller T, Howe CJ, Knowles TP. Enhancing power density of biophotovoltaics by decoupling storage and power delivery. *Nature Energy* **3**, 75 (2018).

19. Efrati A, Lu C-H, Michaeli D, Nechushtai R, Alsaoub S, Schuhmann W, Willner I. Assembly of photo-bioelectrochemical cells using photosystem I-functionalized electrodes. *Nature Energy* **1**, 15021 (2016).

20. Ravi SK, Swainsbury DJ, Singh VK, Ngeow YK, Jones MR, Tan SC. A Mechanoresponsive Phase-Changing Electrolyte Enables Fabrication of High-Output Solid-State Photobioelectrochemical Devices from Pigment-Protein Multilayers. *Advanced Materials* **30**, 1704073 (2018).

21. Yehezkeli O, Tel-Vered R, Wasserman J, Trifonov A, Michaeli D, Nechushtai R, Willner I. Integrated photosystem II-based photo-bioelectrochemical cells. *Nature Communications* **3**, 742 (2012).

22. Wang F, Liu X, Willner I. Integration of Photoswitchable Proteins, Photosynthetic Reaction Centers and Semiconductor/Biomolecule Hybrids with Electrode Supports for Optobioelectronic Applications. *Advanced Materials* **25**, 349-377 (2013).

23. Operamolla A, Ragni R, Milano F, Tangorra RR, Antonucci A, Agostiano A, Trotta M, Farinola G. "Garnishing" the photosynthetic bacterial reaction center for bioelectronics. *Journal of Materials Chemistry C* **3**, 6471-6478 (2015).

24. Milano F, Punzi A, Ragni R, Trotta M, Farinola GM. Photonics and Optoelectronics with Bacteria: Making Materials from Photosynthetic Microorganisms. *Advanced Functional Materials*, 1805521 (2018).

25. Pinhassi RI, Kallmann D, Saper G, Dotan H, Linkov A, Kay A, Liveanu V, Schuster G, Adir N, Rothschild A. Hybrid bio-photo-electro-chemical cells for solar water splitting. *Nature communications* **7**, 12552 (2016).

26. Magis GJ, den Hollander M-J, Onderwaater WG, Olsen JD, Hunter CN, Aartsma TJ, Frese RN. Light harvesting, energy transfer and electron cycling of a native photosynthetic membrane adsorbed onto a gold surface. *Biochimica et Biophysica Acta (BBA)-Biomembranes* **1798**, 637-645 (2010).

27. Kornienko N, Zhang JZ, Sakimoto KK, Yang P, Reisner E. Interfacing nature's catalytic machinery with synthetic materials for semi-artificial photosynthesis. *Nature nanotechnology* **13**, 890 (2018).

28. King PW. Semi-synthetic strategy. *Nature Energy* **3**, 921-922 (2018).

29. Sokol KP, Robinson WE, Warnan J, Kornienko N, Nowaczyk MM, Ruff A, Zhang JZ, Reisner E. Bias-free photoelectrochemical water splitting with photosystem II on a dye-sensitized photoanode wired to hydrogenase. *Nature Energy* **3**, 944 (2018).

30. Zhang H, Liu H, Tian Z, Lu D, Yu Y, Cestellos-Blanco S, Sakimoto KK, Yang P. Bacteria photosensitized by intracellular gold nanoclusters for solar fuel production. *Nature nanotechnology* **13**, 900 (2018).

31. Sawa M, Fantuzzi A, Bombelli P, Howe CJ, Hellgardt K, Nixon PJ. Electricity generation from digitally printed cyanobacteria. *Nature Communications* **8**, 1327 (2017).

32. Mirvakili SM, Slota JE, Usgaocar AR, Mahmoudzadeh A, Jun D, Mirvakili MN, Beatty JT, Madden JDW. Photoactive Electrodes Incorporating Electrosprayed Bacterial Reaction Centers. *Advanced Functional Materials* **24**, 4789-4794 (2014).

33. Ham M-H, Choi JH, Boghossian AA, Jeng ES, Graff RA, Heller DA, Chang AC, Mattis A, Bayburt TH, Grinkova YV. Photoelectrochemical complexes for solar energy conversion that chemically and autonomously regenerate. *Nature Chemistry* **2**, 929-936 (2010).

34. den Hollander M-J, Magis JG, Fuchsenberger P, Aartsma TJ, Jones MR, Frese RN. Enhanced Photocurrent Generation by Photosynthetic Bacterial Reaction Centers through Molecular Relays, Light-Harvesting Complexes, and Direct Protein-Gold Interactions. *Langmuir* **27**, 10282-10294 (2011).

35. Sumino A, Dewa T, Sasaki N, Kondo M, Nango M. Electron conduction and photocurrent generation of a light-harvesting/reaction center core complex in lipid membrane environments. *The journal of physical chemistry letters* **4**, 1087-1092 (2013).

36. Swainsbury DJ, Friebe VM, Frese RN, Jones MR. Evaluation of a biohybrid photoelectrochemical cell employing the purple bacterial reaction centre as a biosensor for herbicides. *Biosensors and Bioelectronics* **58**, 172-178 (2014).

37. Yaghoubi H, Li Z, Jun D, Lafalce E, Jiang X, Schlaf R, Beatty JT, Takshi A. Hybrid Wiring of the Rhodobacter sphaeroides Reaction Center for Applications in Bio-photoelectrochemical Solar Cells. *The Journal of Physical Chemistry C* **118**, 23509-23518 (2014).

38. Caterino R, Csiki R, Lyuleeva A, Pfisterer J, Wiesinger M, Janssens SD, Haenen K, Cattani-Scholz A, Stutzmann M, Garrido JA. Photocurrent generation in diamond electrodes modified with reaction centers. *ACS applied materials & interfaces* **7**, 8099-8107 (2015).

39. Gebert J, Reiner-Rozman C, Steininger C, Nedelkovski V, Nowak C, Wraight CA, Naumann RL. Electron Transfer to Light-Activated Photosynthetic Reaction Centers from Rhodobacter sphaeroides Reconstituted in a Biomimetic Membrane System. *The Journal of Physical Chemistry C* **119**, 890-895 (2015).

40. Friebe VM, Delgado JD, Swainsbury DJ, Gruber JM, Chanaewa A, van Grondelle R, von Hauff E, Millo D, Jones MR, Frese RN. Plasmon-Enhanced Photocurrent of Photosynthetic Pigment Proteins on Nanoporous Silver. *Advanced Functional Materials* **26**, 285-292 (2016).

41. Yaghoubi H, Lafalce E, Jun D, Jiang X, Beatty JT, Takshi A. Large Photocurrent Response and External Quantum Efficiency in Biophotoelectrochemical Cells Incorporating Reaction Center Plus Light Harvesting Complexes. *Biomacromolecules* **16**, 1112-1118 (2015).

42. Kondo M, Iida K, Dewa T, Tanaka H, Ogawa T, Nagashima S, Nagashima KVP, Shimada K, Hashimoto H, Gardiner AT, Cogdell RJ, Nango M. Photocurrent and Electronic Activities of Oriented-His-Tagged Photosynthetic Light-Harvesting/Reaction Center Core Complexes Assembled onto a Gold Electrode. *Biomacromolecules* **13**, 432-438 (2012).

43. Das R, Kiley PJ, Segal M, Norville J, Yu AA, Wang LY, Trammell SA, Reddick LE, Kumar R, Stellacci F, Lebedev N, Schnur J, Bruce BD, Zhang SG, Baldo M. Integration of photosynthetic protein molecular complexes in solid-state electronic devices. *Nano Letters* **4**, 1079-1083 (2004).

44. LeBlanc G, Chen G, Gizzie EA, Jennings GK, Cliffel DE. Enhanced Photocurrents of Photosystem I Films on p-Doped Silicon. *Advanced Materials* **24**, 5959-5962 (2012).

45. Singh VK, Ravi SK, Ho JW, Wong JKC, Jones MR, Tan SC. Biohybrid photoprotein-semiconductor cells with deep-lying redox shuttles achieve a 0.7 V photovoltage. *Advanced Functional Materials* **28**, 1703689 (2018).

46. Mershin A, Matsumoto K, Kaiser L, Yu D, Vaughn M, Nazeeruddin MK, Bruce BD, Graetzel M, Zhang S. Self-assembled photosystem-I biophotovoltaics on nanostructured TiO2 and ZnO. *Scientific reports* **2**, (2012).

47. Yaghoubi H, Schaefer M, Yaghoubi S, Jun D, Schlaf R, Beatty JT, Takshi A. A ZnO nanowire bio-hybrid solar cell. *Nanotechnology* **28**, 054006 (2017).

48. Jung H, Gulis G, Gupta S, Redding K, Gosztola DJ, Wiederrecht GP, Stroscio MA, Dutta M. Optical and electrical measurement of energy transfer between nanocrystalline quantum dots and photosystem I. *The Journal of Physical Chemistry B* **114**, 14544-14549 (2010).

49. Yang Y, Gobeze HB, D'Souza F, Jankowiak R, Li J. Plasmonic Enhancement of Biosolar Cells Employing Light Harvesting Complex II Incorporated with Core-Shell Metal@TiO2Nanoparticles. *Advanced Materials Interfaces* **3**, 1600371 (2016).

50. Ravi SK, Yu Z, Swainsbury DJ, Ouyang J, Jones MR, Tan SC. Enhanced Output from Biohybrid Photoelectrochemical Transparent Tandem Cells Integrating Photosynthetic Proteins Genetically Modified for Expanded Solar Energy Harvesting. *Advanced Energy Materials* **7**, 1601821 (2017).

51. Wong EL, Winchester AJ, Pareek V, Madéo J, Man MK, Dani KM. Pulling apart photoexcited electrons by photoinducing an in-plane surface electric field. *Science advances* **4**, eaat9722 (2018).

52. Ravi SK, Sun W, Nandakumar DK, Zhang Y, Tan SC. Optical manipulation of work function contrasts on metal thin films. *Science advances* **4**, eaao6050 (2018).

53. Alarco P-J, Abu-Lebdeh Y, Abouimrane A, Armand M. The plastic-crystalline phase of succinonitrile as a universal matrix for solid-state ionic conductors. *Nature materials* **3**, 476-481 (2004).

54. Hwang D, Kim DY, Jo SM, Armel V, MacFarlane DR, Kim D, Jang S-Y. Highly efficient plastic crystal ionic conductors for solid-state dye-sensitized solar cells. *Scientific Reports* **3**, 3520 (2013).

55. Zhang Q, Liu K, Ding F, Li W, Liu X, Zhang J. Safety-Reinforced Succinonitrile-Based Electrolyte with Interfacial Stability for High-Performance Lithium Batteries. *ACS Applied Materials & Interfaces* **9**, 29820-29828 (2017).

56. Liu J, Friebe VM, Swainsbury DJ, Crouch LI, Szabo DA, Frese RN, Jones MR. Engineered photoproteins that give rise to photosynthetically-incompetent bacteria are effective as photovoltaic materials for biohybrid photoelectrochemical cells. *Faraday discussions* **207**, 307-327 (2018).

57. Siebert CA, Qian P, Fotiadis D, Engel A, Hunter CN, Bullough PA. Molecular architecture of photosynthetic membranes in Rhodobacter sphaeroides: the role of PufX. *The EMBO journal* **23**, 690-700 (2004).

58. Jones MR, Heer-Dawson M, Mattioli TA, Hunter CN, Robert B. Site-specific mutagenesis of the reaction centre from Rhodobacter sphaeroides studied by Fourier transform Raman spectroscopy: mutations at tyrosine M210 do not affect the electronic structure of the primary donor. *FEBS letters* **339**, 18-24 (1994).

Acknowledgments

S.C.T. acknowledges financial support from MOE AcRF 1 (R-284-000-161-114). M.R.J. acknowledges support from the Biotechnology and Biological Sciences Research Council (BBSRC—project BB/I022570/1) and the BrisSynBio Synthetic Biology Research Centre at the University of Bristol (BB/L01386X/1) funded by the BBSRC and the Engineering and Physical Sciences Research Council (EPSRC) of the UK.

S.K.R. thanks Dr. Fangfang Zhao, Bruker Nano Surfaces and NUS undergraduates Fanrui Hu and Dandan Zhu for their assistance in the experiments.

Author contributions:

S.K.R. and S.C.T. conceived the concept presented and designed the experiments. M.R.J. provided the biological materials. S.K.R concocted the gel electrolyte. Y.Z. and Y.W., contributed to the experimental design and discussion of the study. S.K.R. performed the electrical and rheological measurements. The experiments were, in part, performed in the laboratories of, and in collaboration with, W.S.

S.K.R. and D.K.N. performed the KPFM measurements. S.K.R. M.R.J. and S.C.T. analyzed and interpreted the data and wrote the manuscript. S.C.T. supervised the project.

Competing interests:

The authors declare that they have no competing interests.

Figures:

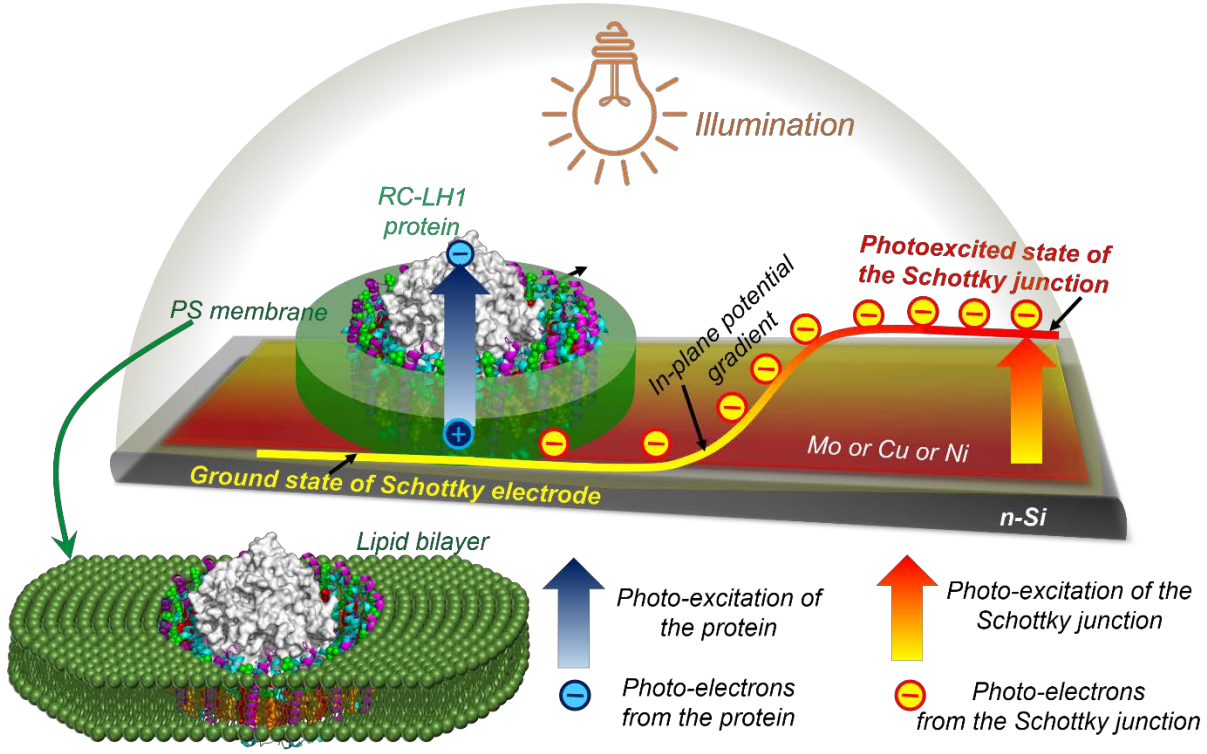

Figure 1: **Schematic of a Bio-Schottky electrode.** A metal/n-Si Schottky junction electrode is partially covered by a highly-absorbing film of *Rba. sphaeroides* photosynthetic (PS) membranes containing RC-LH1 complexes. Electrons and holes generated as a result of charge separation in the RCs are shown in blue/cyan and electrons generated in the Schottky junction are shown in red/yellow. The Schottky electrode surface exhibits a lateral potential gradient between exposed and covered areas.

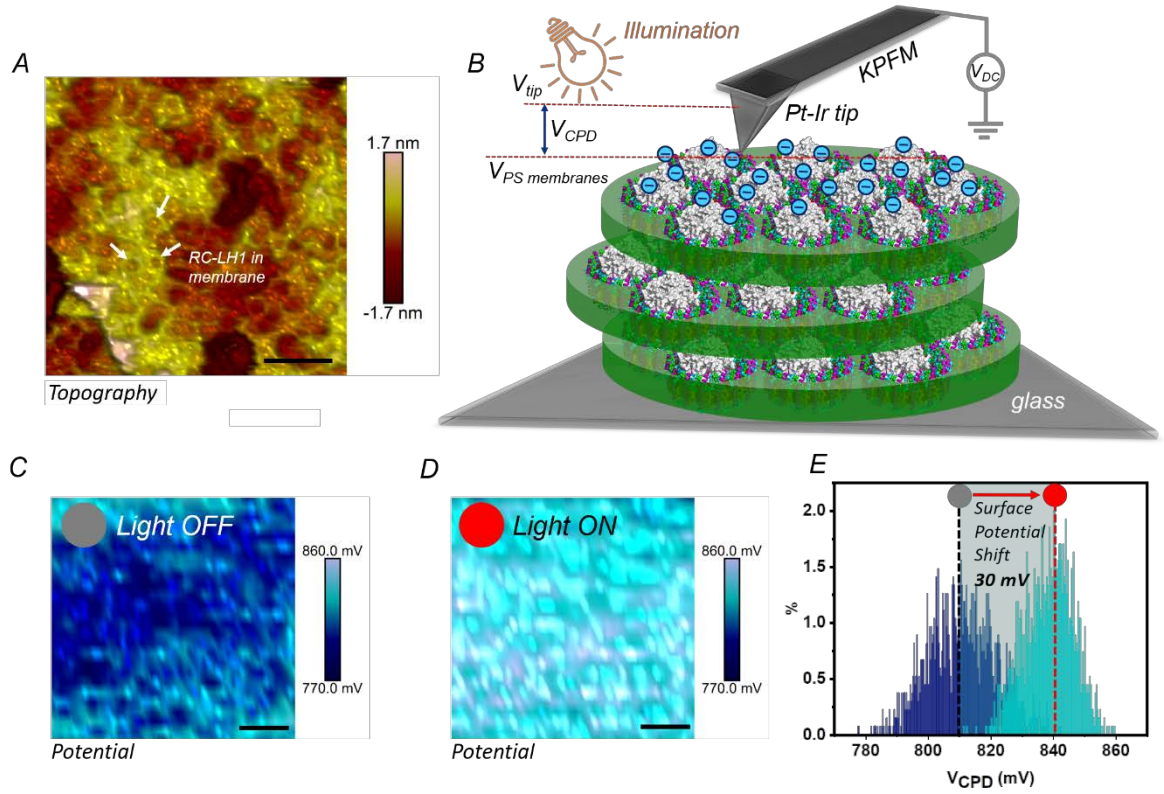

Figure 2: Topological and photo-electric characteristics of the photosynthetic membrane film: (A) AFM topography of a drop-cast and vacuum-dried film of RC-LH1 photosynthetic membranes. Arrows indicate circular features of diameter consistent with RC-LH1 complexes. (B) Schematic of surface potential characterization of photosynthetic membrane multilayers using KPFM with in-situ illumination. In reality the orientation of membrane fragments will be random within the multilayer film. (C-D) Contact potential difference map of a membrane film in the dark (C) and under illumination (D). (E) Histograms of contact potential difference measured over the 40,000 nm^2 area. A shift of 30 mV occurs upon illumination, measured between the mode values of the two distributions (dotted lines). In (A), (C) and (D) the scale bars represent 40 nm.

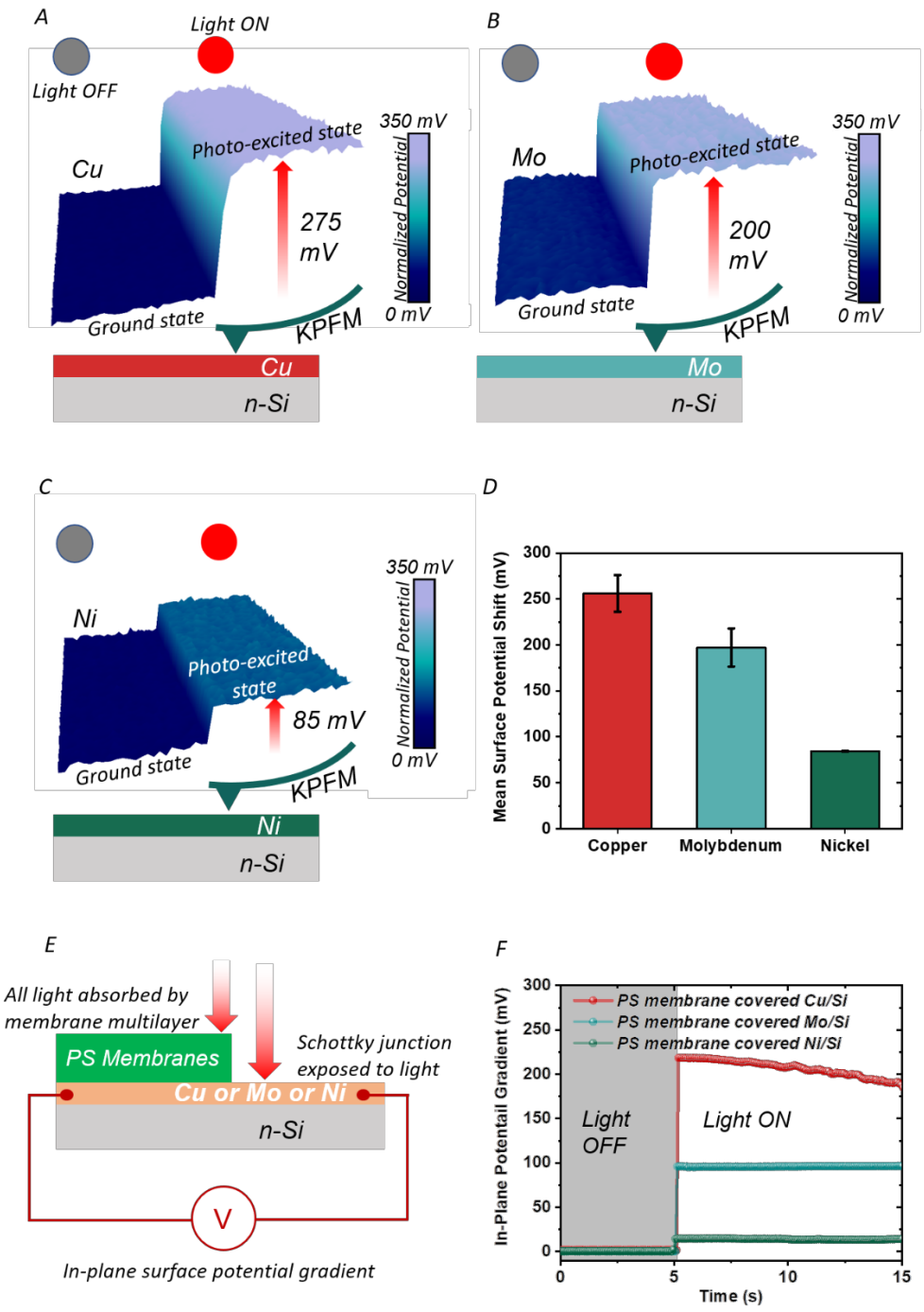

Figure 3: **Characteristics of Schottky electrodes.** (A-C) Change in contact potential difference on illumination measured over an area of 40,000 nm^2 by KPFM for (A) Cu-coated n-Si, (B) Mo-coated n-Si and (C) Ni-coated n-Si. (D) Mean illumination-induced surface potential shift for the three electrodes; the data points are averages of individual mode-to-mode potential shifts from at least three measurements with error bars representing the standard error. (E) Schematic of measurement of an in-plane surface potential gradient after coating part of the metal surface with a photosynthetic membrane film. (F) In-plane potential gradients in the dark and in the light for the three partially-coated Schottky electrodes.

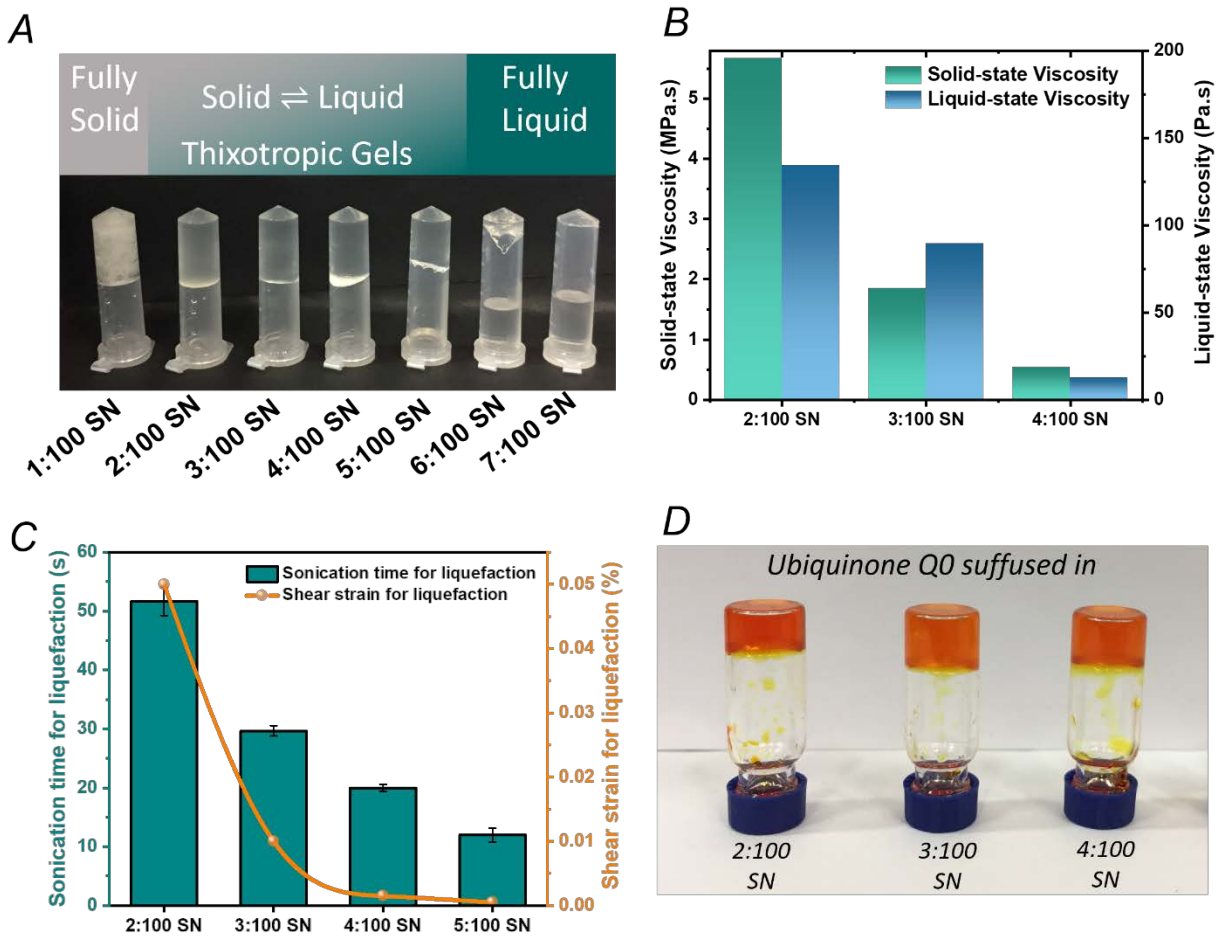

Figure 4: Synthesis and characterization of thixotropic gel electrolytes. (A) Addition of small volumes of water to molten succinonitrile (SN) followed by ambient air cooling produced mixtures that were either fully solid, liquid or underwent a thixotropic solid ↔ liquid phase transition by sonicating and resting. Mixtures with a water:SN volume fraction ranging from 2:100 to 4:100 were fully phase-reversible. (B) Viscosities of the thixotropic mixtures in the solid and liquid states. (C) Sonication times and shear strains required for liquefying the thixotropic gels; the sonication times are the average values from three replicates with error bars representing the standard error. (D) Q0-SN electrolyte gels with a stable solid phase; Q0 had a final concentration of 80 mM.

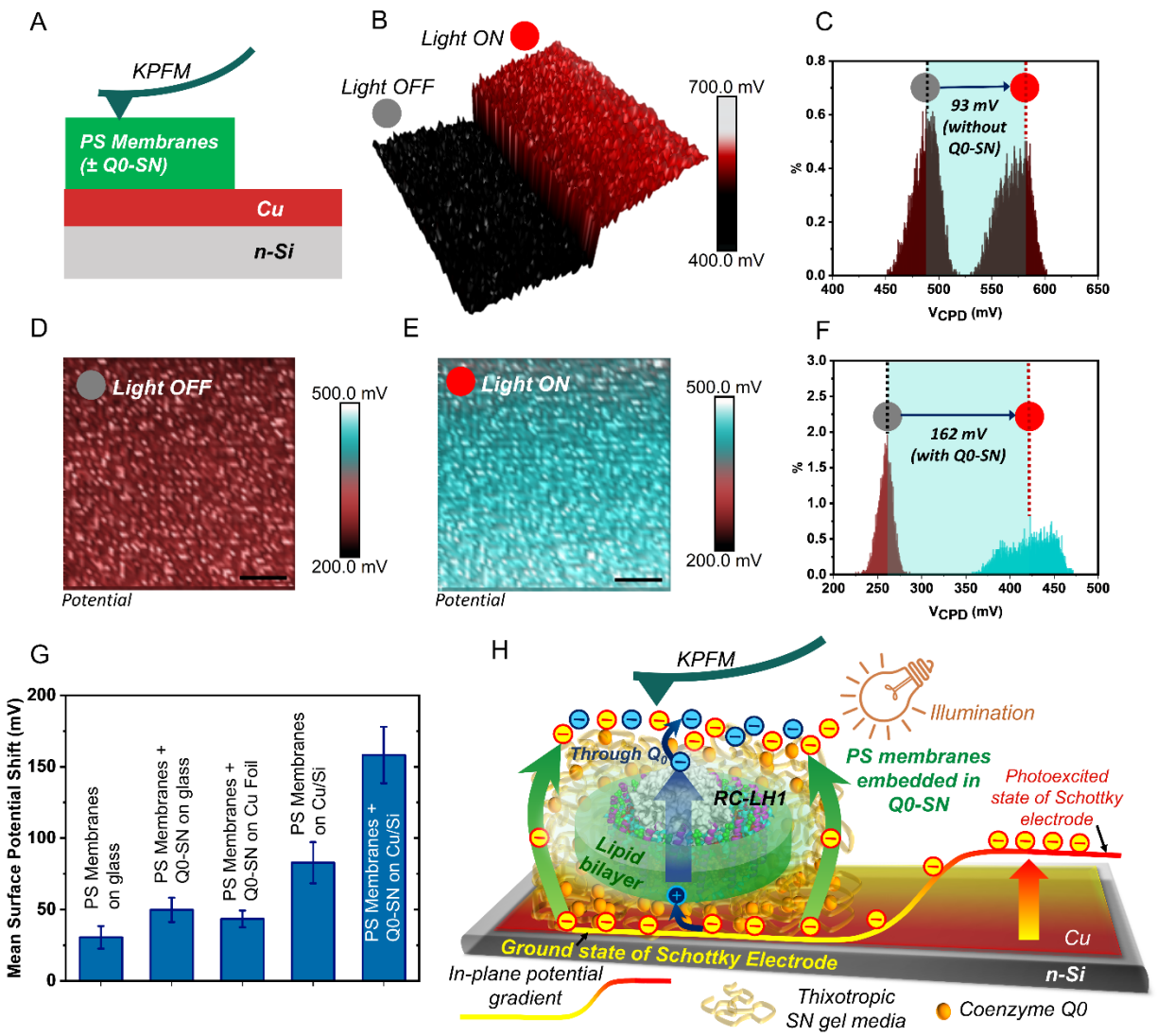

Figure 5: Role of the electrolyte in enhancing light-induced surface potential shifts. (A) Schematic showing the surface potential characterization of a Cu/Si Schottky photoelectrode partially coated with a photosynthetic membrane film with or without an electrolyte. (B) KPFM map showing change in contact potential difference for the surface of a membrane patch (without electrolyte) on a Cu/Si substrate upon illumination; scan area: 40,000 nm^2. (C) Histogram of contact potential difference over the scanned area showing a mode-to-mode shift of 93 mV upon illumination. (D-E) KPFM maps of a membrane/Q0-SN composite film on a Cu/Si electrode showing the surface potential in dark (D) and under illumination (E). (F) Corresponding histogram showing a mode-to-mode shift of 162 mV on illumination. (G) Mean surface potential shifts in different photoelectrodes with and without Schottky junctions and electrolyte; the data points are averages of mode-to-mode potential shifts from at least three measurements with error bars representing a standard deviation. (H) Schematic showing the generation of an in-plane potential gradient and its translation across the device as a result of charge transport through the membrane multilayer by the electrolyte. In (D) and (E) the scale bars represent 40 nm.

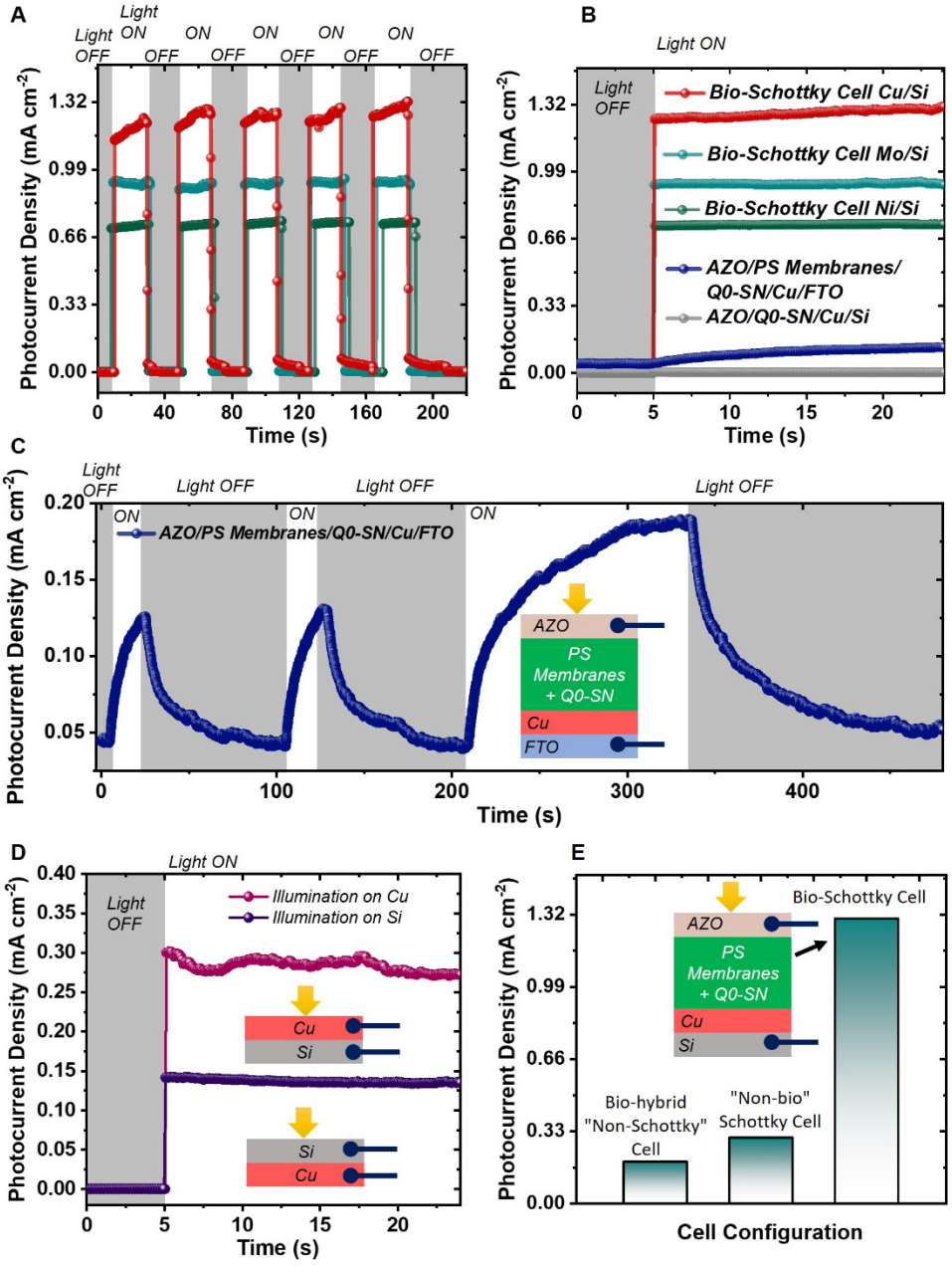

Figure 6: Photocurrent generation by Bio-Schottky and control cells. (A) Photocurrents from Bio-Schottky cells in response to ~20 s light-on/light-off cycles (timing of light-on/light-off is shown for the Cu/Si cell). (B) Photocurrents from Bio-Schottky cells compared to a control Cu/Si cell without the photosynthetic membrane film and a control "non-Schottky" cell where the Schottky junction was replaced by Cu/FTO-glass substrate. (C) The small photocurrents in the cell lacking the Schottky junction showed slow rise and decay times. (D) Photocurrents from a "non-bio" Schottky cell illuminated either from the Cu or n-Si side. (E) Summary of the synergistic effect seen with the Bio-Schottky cells of combining the metal/n-Si Schottky junction with the membrane/Q0-SN multilayer.

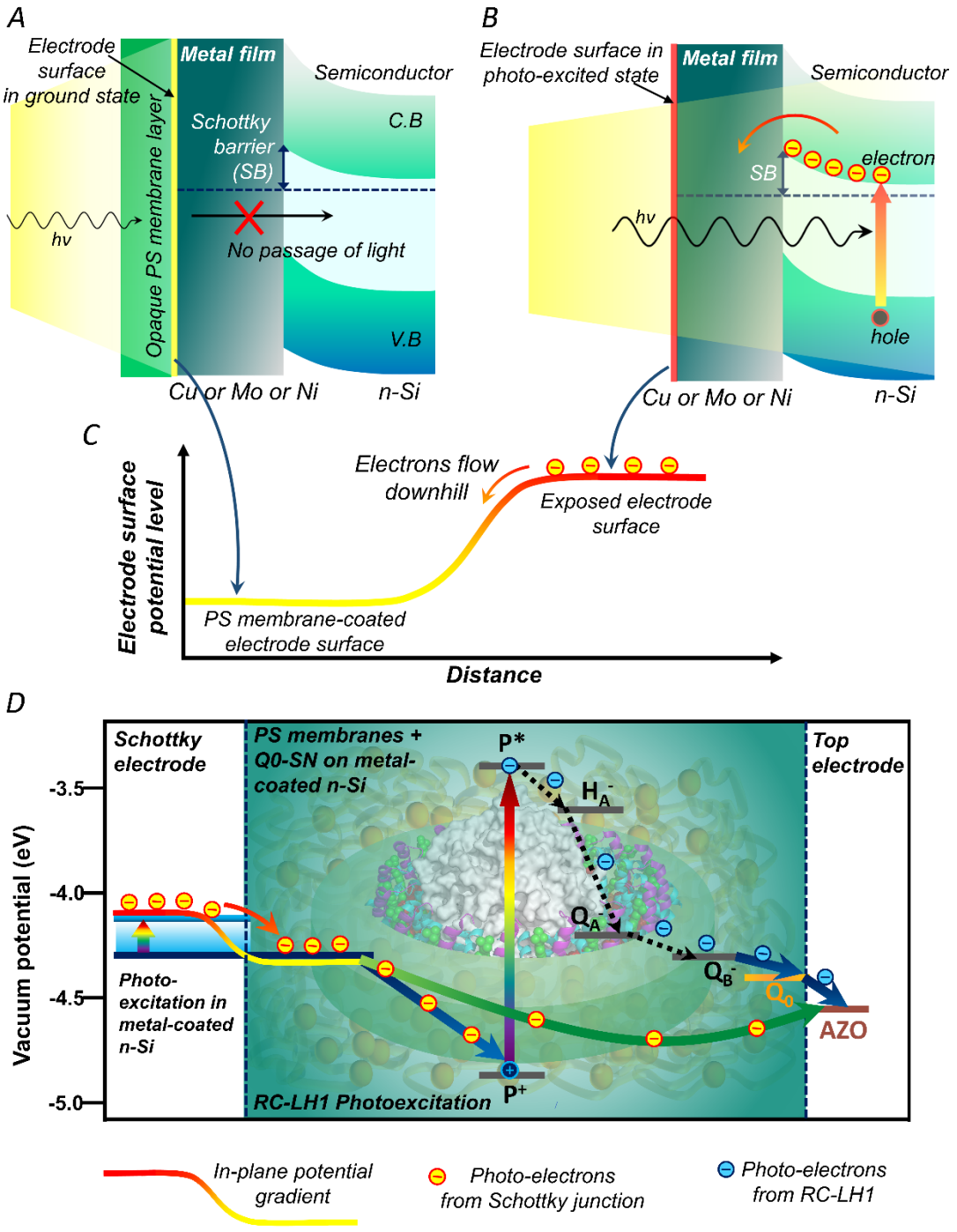

Figure 7: Proposed mechanism of the Bio-Schottky Cell. (A) In coated areas of the metal thin film an opaque multilayer of photosynthetic membrane absorbs all incident light and prevents the photoexcitation of underlying n-Si, such that electrons in the metal surface layer remain in ground state. (B) In uncoated areas photo-excited electrons are injected from the conduction band of the semiconductor into the surface metal thin film. (C) A Schottky electrode partly coated with an opaque layer of photosynthetic membrane with an equal area exposed to light has a surface potential gradient that drives a down-hill electron flow. (D) Energy level diagram corresponding to the working mechanism of the Bio-Schottky cell. The Q0 electrolyte is held in an SN plastic crystalline matrix and facilitates electron transfer across the RC-LH1 membrane multilayer.